Spaceborne SAR Antenna Size Reduction Enabled by Compressive Sampling

Xiaqing (Valerie) Yang, Vishal M. Patel and Athina P. Petropulu,
Department of Electrical and Computer Engineering
Rutgers, the State University of New Jersey, Piscataway, New Jersey, 08854, USA
{xiaqing.yang, vishal.m.patel, athinap}@rutgers.edu

***Abstract*—In synthetic aperture radar (SAR) systems the antenna size needs to meet a minimum requirement in order for range and azimuth ambiguities to be avoided. This paper demonstrates that, by using random or jittered undersampling in the slow-time axis followed by sparse signal recovery techniques, one can reduce the SAR antenna size beyond that minimum requirement without significant loss target estimation performance. In other words, compressive sampling can enable compression of the physical interface in addition to the well cited benefits for data reduction.**

I. Introduction

Synthetic aperture radar (SAR) is a coherent radar imaging system, which utilizes the flight path of the platform to simulate an extremely large aperture and thus generate high-resolution images of terrain and targets [1], [2]. One of the main advantages of SAR is its ability to operate in all weather conditions. There are essentially three main types of SAR - spotlight mode, stripmap mode and scan mode. In spotlight mode SAR, the radar sensor steers its antenna beam to continuously illuminate the terrain patch of interest. SAR - spotlight mode can provide higher resolution than stripmap and scan mode SAR because it maps a scene at multiple viewing angles during a single pass [2]. For example, one can achieve a spatial resolution of 0.05 meters by operating in spotlight mode using a 3GHz bandwidth signal.

When designing a SAR system, antenna size (height and width) is an important parameter. In order to avoid range and azimuth ambiguities, a minimum SAR antenna area constraint is imposed [4]–[6]. Meeting that size constraint comes at high hardware cost. As an example, the spaceborne SAR antennas are typically large $9-15$ m in width (azimuth dimension) and $0.6-4$ m in height (elevation dimension) which are costly to build and deploy [6].

In recent years, compressive sampling (CS) methods [7], [8] have been applied to SAR imaging in which the sparsity of targets in the range-azimuth domain is exploited to reduce the sampling rate in slow and/or fast time [3], [10], [11], [17]. In particular, random and jittered slow-time undersampling methods were proposed in [3] for compressive SAR imaging. It was shown in [3] that this undersampling scheme may not only produce high quality images, but can also enable imaging of much wider swaths, and reduction of storage requirements.

This work was supposed by NSF under grant 1408437.

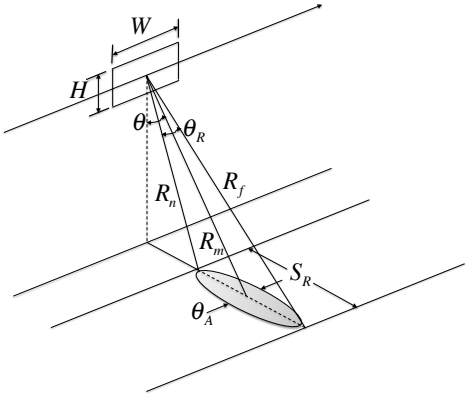

Fig. 1: An imaging geometry for a spotlight mode SAR.

In this paper we consider a spaceborne SAR system operating in spotlight mode with wideband waveforms. Using the CS methods proposed in [3], we show that one can decrease the SAR antenna size beyond what is required by the minimum antenna area constraint without significant loss in the signal-to-noise ratio (SNR). More specifically, we show that by manipulating the pulse repetition frequency (PRF) of the radar, one can decrease the SAR antenna height by the average slow-time undersampling factor.

The remainder of this paper is organized as follows. Section II, presents the SAR ambiguity analysis in terms of PRF and minimum antenna area constraint. In Section III, we describe how CS can be used to reduce the minimum SAR antenna size in detail. Numerical simulations are provided in Section IV. Finally, Section V concludes this paper with a brief summary and discussion.

II. Ambiguity Analysis

A spaceborne SAR antenna of width W and height H, traveling at a constant velocity v in a straight path, pointed orthogonal to the flight path illuminates the ground region with the range swath length S_R, as shown in Fig. 1. The SAR generates linear frequency modulation (LFM) beams whose angular range 3dB beamwidth of antenna and azimuth 3dB beamwidth of antenna are θ_R and θ_A, respectively.

The radar beam intercepts the ground at near range R_n and

far range R_f, giving the ground range swath

$$S_R \approx \frac{R_f - R_n}{\sin(\theta)}, \tag{1}$$

where θ denotes the angle of incidence [4]. To avoid range ambiguity, it is required that the earliest possible echo from any point within the illuminated scene due to the nth pulse transmission is received after the last possible echo due to the $n-1$th pulse transmission [12], i.e.,

$$\frac{2R_f}{c} \leq \frac{2R_n}{c} + \text{PRI}, \tag{2}$$

where PRI denotes the pulse repetition interval, which equals the inverse PRF, and c is the speed of light. Combining (1) and (2), we can lower-bound the PRI by

$$\text{PRI} \geq \frac{2(R_f - R_n)}{c} = \frac{2S_R \sin(\theta)}{c}. \tag{3}$$

The 3dB range angular beamwidth is defined as $\theta_R = \frac{\lambda}{H}$ [5], and can be approximated as

$$\frac{\lambda}{H} = \theta_R \approx \frac{S_R \cos(\theta)}{R_m}, \tag{4}$$

where λ is the wavelength and S_R denotes the range swath. Combing (3) and (4), we can achieve a new lower bound for the PRI as

$$\text{PRI} \geq \frac{2\lambda R_m \sin(\theta)}{cH\cos(\theta)}. \tag{5}$$

The 3dB azimuth angular beamwidth is defined as $\theta_A = \frac{\lambda}{W}$, the synthetic aperture length is $L_s = \theta_A R_m = \frac{\lambda}{W} R_m$ and the synthetic aperture time is $T_s = \frac{L_s}{v}$. With the doppler frequency rate equal to $f_r = \frac{2v^2}{\lambda R_m}$ and the azimuth bandwidth $B_a = f_r T_s = \frac{2v}{W}$, the azimuth resolution is given $R_a = \frac{v}{B_a} = \frac{W}{2}$. Thus, to avoid the azimuth ambiguities, the PRF needs to satisfy

$$\text{PRF} \geq \frac{v}{R_a}$$

which gives the upper bound of the PRI

$$\text{PRI} \leq \frac{W}{2v}. \tag{6}$$

With (5) and (6), to avoid the range and azimuth ambiguities, the PRI is constrained by the following inequalities

$$\frac{2\lambda R_m \sin(\theta)}{cH\cos(\theta)} \leq \text{PRI} \leq \frac{W}{2v}. \tag{7}$$

The minimum size of the antenna can thus be obtained as

$$A_{\min} = WH \geq \frac{4v\lambda R_m \sin(\theta)}{c\cos(\theta)}. \tag{8}$$

For a given azimuth bandwidth B, based on the Nyquist sampling theorem and to avoid aliasing, the following has to hold

$$B \leq \frac{1}{2T_i} = \frac{1}{2v\text{PRI}_{NYQ}}, \tag{9}$$

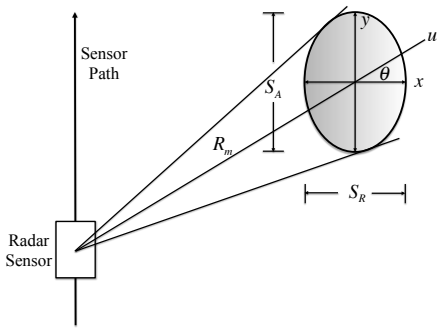

Fig. 2: A ground-plane geometry for a spotlight mode SAR.

where T_i denotes the sampling interval in azimuth and PRI_{NYQ} the Nyquist PRI, which satisfies

$$\text{PRI}_{NYQ} \in \left[\frac{2\lambda R_m \sin(\theta)}{cH\cos(\theta)}, \frac{W}{2v}\right]. \tag{10}$$

Since $\text{PRF}_{NYQ} = \frac{1}{\text{PRI}_{NYQ}}$, from (10) the height of the SAR antennas array is constrained by

$$H \geq \frac{2\lambda R_m \text{PRF}_{NYQ} \sin(\theta)}{c\cos(\theta)}. \tag{11}$$

In other words, the minimum of the array height is proportional to the radar PRF.

In the next section, we will show how CS can be used to reduce the SAR antenna size by lowering the average radar PRF.

III. Antenna Size Reduction Based on CS

The ground-plane spotlight mode SAR geometry corresponding to Fig. 1 is shown in Fig. 2. In the spotlight mode, the SAR steers at a fixed scene as the radar sensor traverses the straight path. The transmitted pulse is the real part of

$$f(t) = \exp\left(j(\omega_0 t + \beta t^2/2)\right)\text{rect}(t), \tag{12}$$

where ω_0 and β denote the pulse carrier frequency and chirp rate, t is the fast-time variable in range direction and rect(t) equals one in $[-T_c/2, T_c/2]$ and zero elsewhere with T_c denoting the pulse duration. The return echoes from the scene patch with range and azimuth swath S_R and S_A is first multiplied by the delayed in-phase and quadrature versions of $f(t)$ and then passed through low-pass filters. Assume R_m, which is the range distance between the radar antenna and the center of the swath, is much larger than S_R and S_A and neglect the residual video phase term. Then, the demodulated received echoes which is also known as the phase histories, is given by

$$s_\theta(t) = \int\int_\Gamma \sigma(x,y)\exp\{-j\Omega(t)(x\cos(\theta)+y\sin(\theta))\}dxdy, \tag{13}$$

where θ is the angle of incidence,

$$\Gamma = \left\{(x,y)|\frac{4x^2}{S_R^2} + \frac{4y^2}{S_A^2} \leq 1\right\}, \tag{14}$$

$\Omega(t) = \frac{2}{c}\left(\omega_0 + \beta(t - \frac{2R_m}{c})\right)$, and $\sigma(x,y) \in \mathbb{C}^{N_s \times N_r}$ is the reflectivity profile in which N_s and N_r denote the number of discretized slow-time and fast-time samples, respectively [13]. It can be observed that $s_\theta(t)$ in (13) represents the finite projection slice through the 2-D Fourier transform of $\sigma(x,y)$ at angle θ [13], [18].

One can formulate the above described imaging problem as

$$\mathbf{s} = \mathbf{C}\boldsymbol{\sigma}, \tag{15}$$

where $\mathbf{s} = [\mathbf{s}_{\theta_1}, \mathbf{s}_{\theta_2}, ..., \mathbf{s}_{\theta_{N_s}}]^T$, $\mathbf{s}_{\theta_i}$ is the fast-time samples at the observation angle θ_i, $\boldsymbol{\sigma} \in \mathbb{C}^{N_s N_r \times 1}$ is the lexicographically vectorized discrete reflectivity profile $\sigma(x,y)$ and $\mathbf{C} = [\mathbf{C}_{\theta_1}, \mathbf{C}_{\theta_2}, ..., \mathbf{C}_{\theta_{N_s}}]^T$ is the discrete realization of the observation kernel based on (13) [3]. Note that the SAR observation matrix can be specifically written as

$$\mathbf{C}_{\theta_i}^{m,q} = \exp\{-j\Omega(t_m)(x_q \cos\theta_i + y_q \sin\theta_i)\}, \tag{16}$$

where t_m is the mth, $m = 1, 2, ..., N_r$, sampling instance of the fast-time t and, x_q and y_q denotes the Cartesian coordinates of the qth, $q = 1, 2, ..., N_s N_r$, element of $\boldsymbol{\sigma}$ [14].

In many SAR imaging applications, such as detection of ships or targets on the ocean, the illuminated target scene can be considered sparse. That is, only a small number of pixels in the SAR image have large values and those pixels correspond to targets of interest. With recent developments in the theory and applications of CS, the number of samples needed to reconstruct the target scene can be much lower than the samples that satisfy the Nyquist sampling theorem [3], [17]. Let Φ denote the restriction operator that selects the phase histories, $\mathbf{s}$. In the presence of noise η, one can write the compressive SAR observation model as

$$\tilde{\mathbf{s}} = \Phi\mathbf{s} + \eta = \Phi\mathbf{C}\boldsymbol{\sigma} + \eta. \tag{17}$$

Assume that $\boldsymbol{\sigma}$ has a sparse representation (or is compressible) in some basis Ψ, so that $\boldsymbol{\sigma} = \Psi\alpha$, where α is the sparse coefficient vector corresponding to $\mathbf{s}$ in the basis Ψ. With this, the CS SAR observation model (17) can be rewritten as

$$\tilde{\mathbf{s}} = \Phi\mathbf{C}\Psi\alpha + \eta = \Theta\alpha + \eta, \tag{18}$$

where $\Theta = \Phi\mathbf{C}\Psi$ is the resulting sensing matrix. Then, the SAR reflectivity map $\boldsymbol{\sigma}$ can be recovered via α by solving the following ℓ_1 optimization problem

$$\min_{\alpha} \mu\|\alpha\|_1 + \frac{1}{2}\|\tilde{\mathbf{s}} - \Theta\alpha\|_2^2, \tag{19}$$

provided that certain conditions are met [3], [8], where $\mu > 0$ is a regularization parameter.

It was shown in [3] that the design of a CS undersampling scheme for SAR entails the selection of phase histories such that the mutual coherence of Θ is small. Since truly random undersampling of the phase histories is not practical, two slow-time undersampling schemes were introduced in [3] by essentially modifying the PRF of the radar. These slow-time undersampling schemes were random slow-time undersampling and jittered slow-time undersampling. In jittered slow-time undersampling, the slow-time samples are undersampled uniformly over a rectilinear subspace [15]. The exact position of the respective sample in each rectilinear subspace varies randomly. Specifically, the time jitter in which the nth sample is jittered by an amount ζ_n occurs at time $nT_{jitter} + \zeta_n$, where T_{jitter} is the jittered sampling period and ζ_n are uncorrelated [3]. The jittered slow-time undersampling via CS enables the reduction of the average PRF compared to the Nyquist sampling.

Suppose we apply jittered undersampling in the slow-time axis which is at an average rate $\frac{1}{D}$ times the Nyquist rate, which suggests

$$\text{PRF}_{CS} = \frac{1}{D} \cdot \text{PRF}_{NYQ}, \tag{20}$$

where PRF_{CS} denotes the average value of the compressive pulse repetition frequency. In the case of CS, (11) can be rewritten as

$$H \geq \frac{2\lambda R_m \text{PRF}_{CS} \sin(\theta)}{c\cos(\theta)} \tag{21}$$

$$= \frac{1}{D}\left(\frac{2\lambda R_m \text{PRF}_{NYQ} \sin(\theta)}{c\cos(\theta)}\right). \tag{22}$$

This means one can reduce the antenna height by a factor of D, and be able to reconstruct the image without significant loss of fidelity when using CS for SAR imaging. This has significant impact on the design of various SAR systems.

However, as stated in the radar equations [12], the receive power is proportional to the product of the transmit and receive gains, which is proportional to the power of the antenna size, i.e.,

$$P_r \propto G_t G_r \propto A^2 \propto H^2,$$

where G_t and G_r are the transmit and receive gains and P_r is the receiving power.

Thus, the reduction of the antenna size leads to the diminishing of the receive power which implies the decrease in SNR. In other words, to validate the feasibility of the proposed antenna size reduction method, we need to compare the imaging results with the results at lower SNR scenarios.

IV. Numerical Simulations

In order to validate the feasibility of the proposed antenna size reduction method, we evaluate the performance of the CS SAR imaging algorithms based on jittered slow-time undersampling at different SNRs. As discussed earlier, the slow-time undersampling rate D results in the reduction in antenna size by $\frac{1}{D}$. This results in the loss of SNR by $10\log_{10} D^2$dB. For example, if we reduce the antenna size by half, then we will approximately loose 6dB in SNR.

We use a point target and two closely point targets to generate the phase histories for two simulations. We used the following parameters corresponding to spaceborne SAR in our both simulations: speed of light, $c = 3 \times 10^8$ m/s, center frequency, $f_c = 10^9$ Hz, bandwidth, $B = 6 \times 10^8$ Hz, radar vehicle speed, $v = 7000$ m/s, elevation angle, $\theta = 30^\circ$, the illuminated integration angle, $\triangle\ \theta = 0.5^\circ$, the distance from the initial position of the radar sensor to the center of the

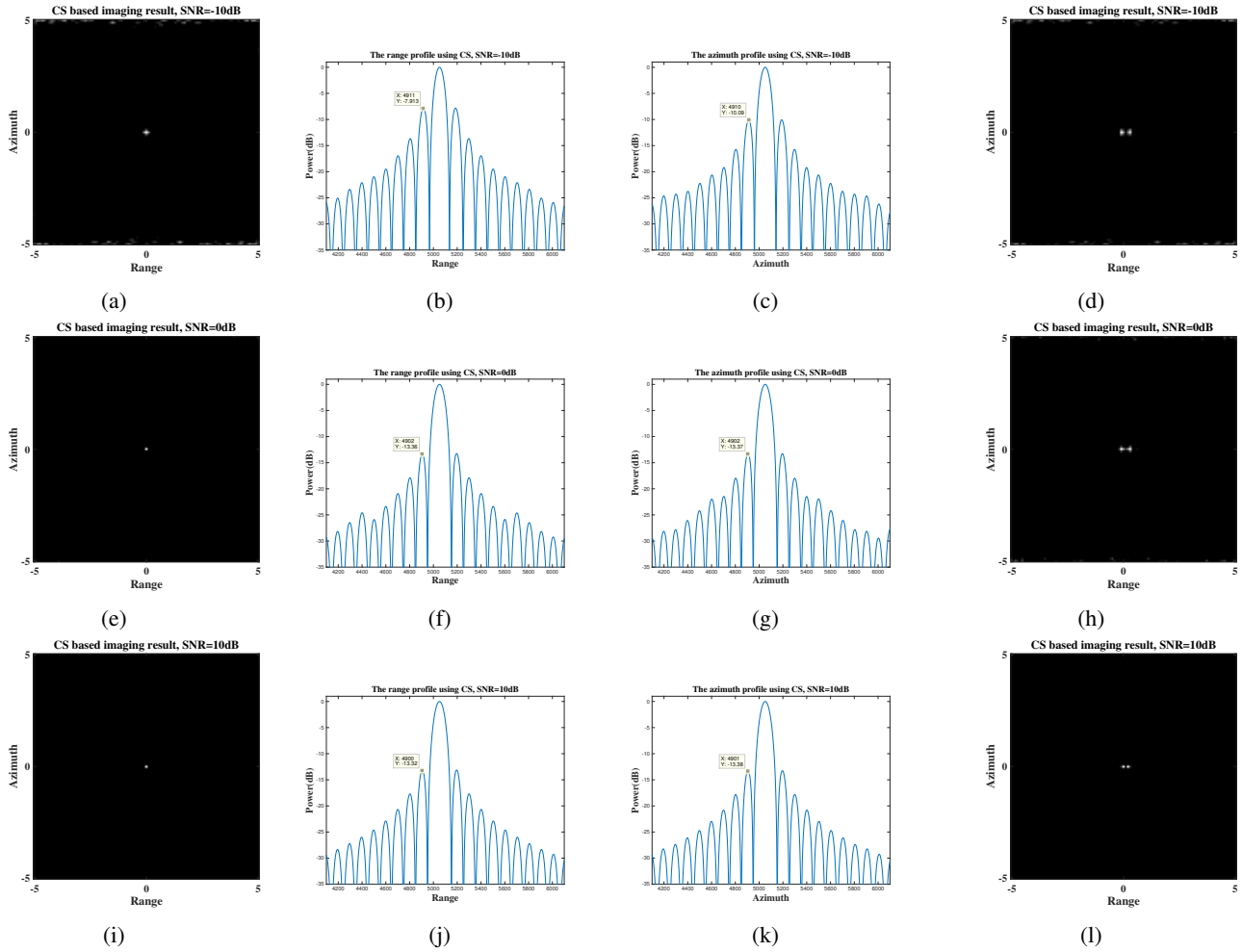

Fig. 3: For a simulated single point target at zero azimuth and range, the first column shows the CS-based imaging results with 50% slow-time undersampled data for SNR=-10dB, SNR=0dB and SNR=10dB. The second column shows the corresponding range profile, and the third column the azimuth profile. The forth column shows the CS-based imaging results with 50% slow-time undersampled data for two very closely simulated point targets at SNR=-10dB, SNR=0dB and SNR=10dB

swath, $R_m = 10^5$ m and the number of discretized fast-time and slow-time samples, $N_r = N_s = 101$.

The CS-based imaging results for single simulated point target with 50% (D=2) slow-time undersampled data at SNR$= -10$dB, SNR$=$ 0dB and SNR$=$ 10dB are shown in Fig. 3(a), Fig. 3(e) and Fig. 3(i), respectively. It can be clearly seen from these figures that the point target can be very well focused when the SNR is above 0dB. Even at very low SNR (e.g. -10dB) the point target is still focused only with the peak side-lobe a little higher than that at 0dB. The imaging results for two very closely spaced simulated point targets also with 50% (D=2) slow-time undersampled data at SNR$= -10$dB, SNR$=$ 0dB and SNR$=$ 10dB are shown in Fig. 3(d), Fig. 3(h) and Fig. 3(l), respectively. It can be observed that for two very closely spaced simulated point targets the imaging results are still good even at low SNRs. It can be concluded from these simulations that the CS-based imaging algorithm can tolerate the noise to a large extent and it can still perform well in the low SNR scenarios. Therefore, it is feasible to reduce the antenna size using CS methods to a certain scale (i.e. reducing it to the half of its original size as shown in this example).

V. Conclusion

In this paper, we developed a method based on CS that allows one to reduce the SAR antenna size beyond what is required by the Minimum SAR Antenna Area Constraint and be able to reconstruct the SAR image without significant loss of fidelity. In particular, we utilized the jittered slow-time random sampling scheme which can reduce the average radar PRF, analyzed the minimum antenna size constraint and verified the feasibility of the antenna size reduction when CS methods are used for SAR imaging.

In the future, we will further analyze how the new antenna design affects swath width, azimuth resolution, range and azimuth ambiguity level, and clutter-and signal-to-noise ratios.

REFERENCES

[1] I. G. Cumming, and F. H. Wong, *Digital processing of synthetic aperture radar data: algorithms and implementation,* Artech house, 2005.

[2] W. G. Carrara, R. S. Goodman, and R. M. Majewski, *Spotlight synthetic aperture radar- Signal processing algorithms,* Norwood, MA: Artech House, 1995.

[3] V. M. Patel, G. R. Easley, D. M. Healy Jr, and R. Chellappa,"Compressed synthetic aperture radar," *Selected Topics in Signal Processing, IEEE Journal of* 4, no. 2, pp. 244-254, 2010.

[4] K. Tomiyasu, "Tutorial review of synthetic-aperture radar (SAR) with applications to imaging of the ocean surface," *Proceedings of the IEEE,* vol. 66, no. 5, pp. 563-583,1978.

[5] K. Tomiyasu, "Performance of a proposed spaceborne synthetic aperture radar with variable antenna height," *Geoscience and Remote Sensing, IEEE Transactions on,* vol. 28, pp. 609-613,1990.

[6] A. Freeman, W. Johnson, B. Huneycutt, R. Jordan, S. Hensley, P. Siqueira, and J. Curlander, "The "myth" of the minimum SAR antenna area constraint," *Geoscience and Remote Sensing, IEEE Transactions on,* vol. 38, no. 1, pp. 320-324, 2000.

[7] D. L. Donoho, "Compressed sensing," *Information Theory, IEEE Transactions on* 52.4, pp. 1289-1306, 2006.

[8] E. J. Cands, "The restricted isometry property and its implications for compressed sensing," *Comptes Rendus Mathematique,* vol. 346, no. 9, pp. 589-592, 2008.

[9] Y. Yu, A. P. Petropulu, and H. V. Poor, "MIMO radar using compressive sampling," *IEEE Journal of Selected Topics in Signal Processing,* vol. 4,no. 1, pp. 146-163, 2010.

[10] W. Wei, X. Zhang, J. Shi and X. Gao, "Sparse reconstruction for SAR imaging based on compressed sensing," *Progress In Electromagnetics Research,* vol. 109, pp. 63-81, 2010.

[11] H. Bu, R. Tao, X. Bai, and J. Zhao,"A novel SAR imaging algorithm based on compressed sensing," *Geoscience and Remote Sensing Letters, IEEE,* vol. 12, no. 5, pp. 1003-1007, 2015.

[12] J. C. Curlander, and R. N. McDonough, *Synthetic aperture radar,* New York, NY, USA: John Wiley & Sons, 1991.

[13] M. Cetin, and W. C. Karl, "Feature-enhanced synthetic aperture radar image formation based on nonquadratic regularization," *Image Processing, IEEE Transactions on,* vol 10, no. 4, pp. 623-631, 2001.

[14] F. Shen, G. Zhao, Z. Liu, G. Shi, and J. Lin, "SAR Imaging With Structural Sparse Representation," *Selected Topics in Applied Earth Observations and Remote Sensing, IEEE Journal of,* vol. 8, no. 8, pp. 3902-3910, 2015.

[15] A. V. Balakrishnan, "On the problem of time jitter in sampling," *Information Theory, IRE Transactions on,* vol. 8, no. 3, pp. 226-236, 1962.

[16] H. S. Shapiro, and R. A. Silverman, "Alias-free sampling of random noise," *Journal of the Society for Industrial and Applied Mathematics,* vol. 8, no. 2, pp. 225-248, 1960.

[17] M. Cetin, I. Stojanovic, O. Onhon, K. Varshney, S. Samadi, W. C. Karl and A. S. Willsky, "Sparsity-Driven Synthetic Aperture Radar Imaging: Reconstruction, autofocusing, moving targets, and compressed sensing," *IEEE Signal Processing Magazine*, vol. 31, no. 4, pp. 27-40, July 2014.

[18] M. D. Desai and W. K. Jenkins, "Convolution backprojection image reconstruction for spotlight mode synthetic aperture radar," *IEEE Transactions on Image Processing*, vol. 1, no. 4, pp. 505-517, Oct 1992.